ELSEVIER

Journal of Photochemistry and Photobiology A: Chemistry 108 (1997) 105–116

Journal of PHOTOCHEMISTRY AND PHOTOBIOLOGY A: CHEMISTRY

$CF_3C(O)Cl$: Temperature-dependent (223–298 K) absorption cross-sections and quantum yields at 254 nm

Richard Meller *, Geert K. Moortgat

Max-Planck-Institut für Chemie, Atmospheric Chemistry Department, Postfach 3060, 55020 Mainz, Germany

Received 2 July 1996; accepted 21 February 1997

Abstract

UV absorption cross-sections of trichloroacetyl chloride ($CF_3C(O)Cl$) have been measured using two different apparatuses with spectral resolutions of 0.05 and 0.2 nm in the wavelength range 200–330 nm at temperatures ranging from 223 to 298 K. Photolysis studies of $CF_3C(O)Cl$ in N_2, air/C_2H_6 mixtures and air have been performed at 254 nm. Quantum yields for the dissociation of $CF_3C(O)Cl$ as a function of pressure and product quantum yields for Cl_2 and CO at 296 K have been determined. The temperature-dependent absorption cross-sections and new quantum yields were used to calculate photodissociation rate-constants for $CF_3C(O)Cl$ at different solar zenith angles as a function of altitude. Temperature effects of the photodissociation rate constants are discussed. © 1997 Elsevier Science S.A.

Keywords: Trichloroacetyl chloride; Absorption cross-sections; Quantum yield; Photolysis products; Atmosphere

1. Introduction

Halogenated carbonyl compounds are produced by atmospheric degradation of halocarbons, initiated by OH radical reactions, in the troposphere. The replacement of chlorofluorocarbons (CFCs) by selected hydrochlorofluorocarbons (HCFCs) and hydrofluorocarbons (HFCs) has necessitated studies of the fate of the degradation products of the latter compounds [1]. The mechanism of degradation of the carbonyl compounds is dependent on their location in the atmosphere. Removal in the stratosphere is largely dominated by photolysis, whereas in the troposphere removal by hydrolysis might compete with reactions with OH radicals or with photolysis [2].

Trifluoroacetyl chloride ($CF_3C(O)Cl$) is of particular interest, since it is formed by degradation of HCFC-123 (CF_3CCl_2H) [1–3]. In order to assess the importance of the photolysis of $CF_3C(O)Cl$, it is necessary to determine photolysis parameters such as absorption cross-sections and quantum yields of the primary product pathways under atmospheric pressure and temperature conditions.

Four possible primary photolysis decomposition pathways have been proposed [4].

$$CF_3C(O)Cl + h\nu \rightarrow CF_3 + CO + Cl \quad (1)$$

$$\rightarrow CF_3C(O) + Cl \quad (2)$$

$$\rightarrow CF_3 + C(O)Cl \quad (3)$$

$$\rightarrow CF_3Cl + CO \quad (4)$$

It is important to determine the yield of CF_3Cl from the pathway represented by Eq. (4) since this might introduce a fully halogenated compound into the stratosphere thus affecting the ODP of the parent compound.

In the present study, temperature-dependent (223–298 K) absorption cross-sections have been determined in the wavelength range 200–330 nm. Photolysis products were determined in N_2, air and air/C_2H_6 mixtures. In addition, quantum yields at 254 nm have been obtained in the pressure range 100–760 torr. With these results, the *J*-values (photodissociation rate constants) for $CF_3C(O)Cl$ were calculated at different zenith angles as a function of altitude.

2. Experimental

2.1. Absorption cross-section experiments

The absorption cross-sections of $CF_3C(O)Cl$ were measured in two different apparatuses, both equipped with monochromator, photomultiplier and diode-array detector, which

* Corresponding author. Fax: +49 6131 305436.

PII S1010-6030(97)00094-4

were described in two recent publications [5,6]. One system (A) implemented a cell of 63 cm optical path-length, whereas the other system (B) was equipped with multi-pass optics, with a base path-length of 120 cm. A total absorption path-length of 980 cm was used in the latter configuration. Both cells were temperature-regulated in the range 223–298 K. Stabilized deuterium lamps ((A) Heraeus 200 W and (B) Hamamatsu 30 W) were used as light sources. For system (A), a 0.6 m Jobin–Yvon monochromator was used with a grating having 2400 groves mm^{-1}; system (B) implemented a 0.5 m B & M monochromator equipped a grating with 600 groves mm^{-1}. Absolute capacitance pressure gauges (MKS, 10 torr range, 0.15% maximum deviation) were used in both set-ups.

Measurements between 200 and 300 nm were carried out in apparatus (A) at pressures ranging from 0.2–4.0 torr. Cell (B) was used for the long-wavelength region of the spectrum (280–330 nm) at pressures varying between 3.0 and 12.0 torr. The entire spectrum was obtained by splining the two individual spectra.

Spectra were calculated from Beer–Lambert's law,

$$\sigma(\lambda,T) = \ln[I_0(\lambda)/I(\lambda)]/lN \quad (5)$$

where σ represents the absorption cross-section (cm^2 $molecule^{-1}$) at wavelength λ (nm) and temperature T (K), l the length (cm) of the optical path in the cell, and N the number density (molecule cm^{-3}) of $CF_3C(O)Cl$; I_0 and I refer to the transmitted light intensity obtained at each diode in the array detector with the cell evacuated and filled, respectively. Recorded spectra were transferred via a detector interface to a computer for further analysis. The reported absorption cross-sections of $CF_3C(O)Cl$ at each temperature were obtained by averaging a minimum of seven independent measurements each at a different pressure.

2.2. Photolysis experiments

Photolysis experiments were carried out at ambient temperatures in a long-path multiple reflection cell (43.2 m optical path for IR and 9.82 m for UV) surrounded with three UV-lamps (Philips) [7]. The reactor was made of quartz glass and was coupled to a Bomem DA8 series FTIR interferometer and a UV absorption system. Infrared emission from a globar source traversed the KBr beam-splitter of the spectrometer and the interference signal was monitored with a Cu–Ge detector, cooled to liquid He temperature. Spectra were recorded with a resolution of 1 cm^{-1} between 450 and 4000 cm^{-1}. The UV part of this apparatus consisted of a 200-W deuterium lamp (Heraeus) and a double monochromator (Jobin–Yvon H 225) equipped with two gratings with 600 lines mm^{-1} blazed at 300 nm. Light detection was accomplished with a photomultiplier (Hamamatsu R 106 UH).

2.3. Materials

IR reference spectra from samples of $CF_3C(O)Cl$, CF_2O (both PCR, purity >97%), CF_3Cl, C_2F_6, (both PCR, purity >98%), $CF_3O_2CF_3$ (Fluorochem, purity >98%), CCl_2O (Matheson purity >99%) and $CF_3O_3CF_3$ were taken for calibration purposes. The commercially obtained chemicals were purified by bulb-to-bulb distillation before use. No contamination could be identified in the IR-absorption spectra. $CF_3O_3CF_3$ was prepared as described by Anderson and Fox [8]. IR spectroscopy revealed a 5% $CF_3O_2CF_3$ impurity in $CF_3O_3CF_3$ [9]; this was taken into account for the correction of the $CF_3O_3CF_3$ reference spectrum.

3. Results and discussion

3.1. UV-absorption cross-sections

The absorption spectra of $CF_3C(O)Cl$ at four different temperatures (T = 298, 273, 248, and 223 K) were measured in both UV-apparatuses. $CF_3C(O)Cl$ displays a structureless absorption spectrum which is due to a $n \rightarrow \Pi^*$ transition between 216 and 330 nm. An absorption maximum of $\sigma = 6.87 \times 10^{-20}$ cm^2 $molecule^{-1}$ is reached at 255 nm. A strong absorption band with a maximum at wavelengths below 200 nm is also evident. A cross-section of 5.00×10^{-19} cm^2 $molecule^{-1}$ was measured at 200 nm.

Fig. 1 illustrates the absorption spectrum of $CF_3C(O)Cl$ at 298 K in the range 200–330 nm, and in Fig. 2 the spectra at 298, 273, 248 and 223 K are presented. In Table 1 numerical values averaged over 2-nm intervals for all temperatures are listed. As expected, the absorption cross-sections decrease with decreasing temperature in the long-wavelength tail region (λ > 280 nm) and again between 200 and 220 nm. The band broadening is due to a change in the population of the rotational–vibration states.

Uncertainties in the measured optical path length, temperature, pressure and absorbance contribute to the overall uncertainty in the measured absorption cross-sections. The errors

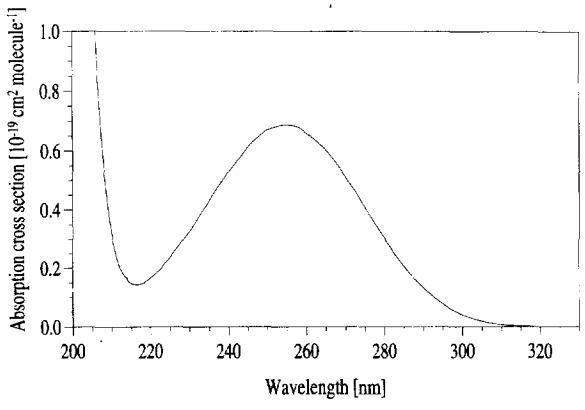

Fig. 1. UV absorption spectrum of $CF_3C(O)Cl$ at 298 K in the range 200–330 nm.

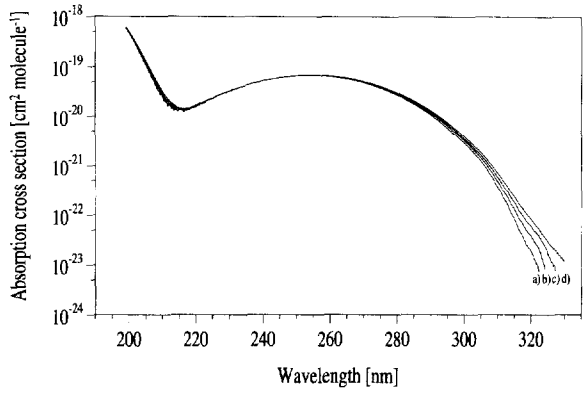

Fig. 2. Absorption spectra of $CF_3C(O)Cl$ at (a) 223 K, (b) 248 K, (c) 273 K and (d) 298 K in the range 200–330 nm.

associated with the measurements of the pressure, temperature and path length amount to about 1%. The accuracy of the absorption measurement was primarily determined by the stability of the output light source (I_0 and I) during the measurement. The overall uncertainty was within $\pm 3\%$ in the wavelength range 200–310 nm, increasing however to 20% at longer wavelengths.

In order to demonstrate the relationship between cross-sections and temperature, the logarithms of the cross-sections at several selected wavelengths ($\lambda = 270, 280, 290, 300, 310$ and 320 nm) were plotted versus temperature as shown in Fig. 3. In this figure it can be seen that the logarithm of the cross-sections changes linearly with temperature. This relationship can be expressed by the equation:

$$\ln\sigma(T) = A(\lambda) + B(\lambda)(T - T_0) \quad (6)$$

where $A(\lambda)$ represents the absorption cross-sections at $T_0 = 273$ K, and $B(\lambda)$ the temperature gradient. The function of the absorption spectrum and the temperature gradient can be expressed by empirical functions according to Eqs. (7) and (8) [10].

$$A(\lambda) = \Sigma a_n \lambda^n = a_0 + a_1\lambda + a_2\lambda^2 + a_3\lambda^3 + a_4\lambda^4 \quad (7)$$

$$B(\lambda) = \Sigma b_n \lambda^n = b_0 + b_1\lambda + b_2\lambda^2 + b_3\lambda^3 + b_4\lambda^4 \quad (8)$$

Eqs. (6)–(8) can be combined in the equation:

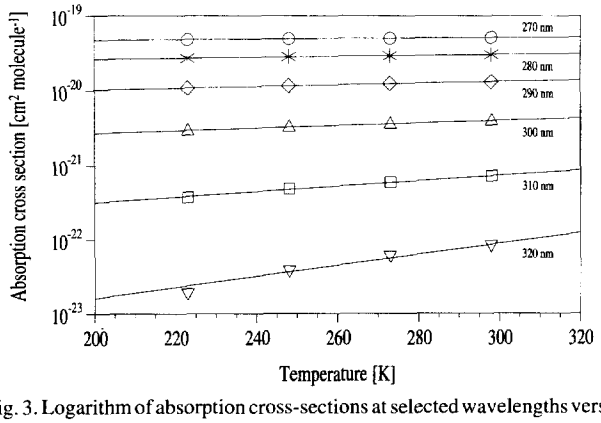

Fig. 3. Logarithm of absorption cross-sections at selected wavelengths versus temperature for $CF_3C(O)Cl$. The lines represent least-square fits.

Table 1
Temperature-dependent absorption cross-section of $CF_3C(O)Cl$

Wavelength (nm)	$10^{20} \times$ Absorption cross section (cm^2 $molecule^{-1}$) at temperature (K):			
	223	248	273	298
200	45.83	47.36	48.70	50.16
202	26.56	27.69	28.87	30.47
204	14.63	15.47	16.37	17.70
206	7.830	8.375	9.016	9.960
208	4.197	4.603	5.001	5.567
210	2.461	2.674	2.907	3.274
212	1.662	1.757	1.903	2.102
214	1.361	1.397	1.496	1.620
216	1.343	1.343	1.386	1.442
218	1.421	1.424	1.449	1.484
220	1.641	1.637	1.632	1.665
222	1.845	1.851	1.893	1.896
224	2.184	2.174	2.195	2.201
226	2.538	2.551	2.524	2.544
228	2.901	2.899	2.908	2.904
230	3.261	3.262	3.251	3.278
232	3.646	3.642	3.647	3.685
234	4.025	4.055	4.052	4.080
236	4.456	4.483	4.485	4.505
238	4.852	4.896	4.869	4.902
240	5.223	5.270	5.258	5.283
242	5.553	5.595	5.580	5.629
244	5.900	5.938	5.912	5.957
246	6.177	6.234	6.212	6.271
248	6.411	6.476	6.433	6.503
250	6.577	6.617	6.611	6.694
252	6.679	6.748	6.709	6.799
254	6.712	6.796	6.762	6.863
256	6.674	6.772	6.744	6.858
258	6.586	6.693	6.677	6.786
260	6.383	6.494	6.486	6.599
262	6.148	6.268	6.272	6.393
264	5.875	6.008	6.025	6.159
266	5.567	5.699	5.724	5.859
268	5.219	5.345	5.377	5.510
270	4.814	4.944	4.985	5.120
272	4.396	4.533	4.590	4.726
274	3.965	4.104	4.169	4.306
276	3.564	3.691	3.758	3.876
278	3.133	3.252	3.323	3.444
280	2.724	2.844	2.922	3.035
282	2.304	2.428	2.516	2.630
284	1.931	2.052	2.146	2.253
286	1.619	1.726	1.812	1.907
288	1.334	1.429	1.506	1.593
290	1.090	1.175	1.249	1.324
292	0.8672	0.9463	1.015	1.082
294	0.6739	0.7443	0.8075	0.8670
296	0.5117	0.5715	0.6271	0.6811
298	0.3977	0.4428	0.4815	0.5282
300	0.2978	0.3335	0.3650	0.4038
302	0.2178	0.2467	0.2717	0.3035
304	0.1520	0.1753	0.1959	0.2214
306	0.1018	0.1205	0.1377	0.1580
308	0.0642	0.0788	0.0927	0.1087
310	0.0376	0.0488	0.0596	0.0722
312	0.0211	0.0293	0.0376	0.0472
314	0.0115	0.0172	0.0232	0.0301
316	0.0061	0.0100	0.0141	0.0189
318	0.0033	0.0060	0.0089	0.0123
320	0.0019	0.0038	0.0060	0.0084
322	–	0.0023	0.0041	0.0057
324	–	–	0.0025	0.0037
326	–	–	0.0013	0.0025
328	–	–	–	0.0017

Table 2
Constants a_i and b_i for the calculation of absorption cross-sections of $CF_3C(O)Cl$ according to Eq. (9) for temperatures from 223 to 298 K and wavelength from 200–220 nm

$a_0 = -2.0111750 \times 10^4$	$b_0 = 3.0306320 \times 10^2$
$a_1 = 3.1757333 \times 10^2$	$b_1 = -5.8082356$
$a_2 = -2.5671017$	$b_2 = 4.1715164 \times 10^{-2}$
$a_3 = 7.8520098 \times 10^{-3}$	$b_3 = -1.3306565 \times 10^{-4}$
$a_4 = -8.9707718 \times 10^{-6}$	$b_4 = 1.5906451 \times 10^{-7}$

Table 3
Constants a_i and b_i for the calculation of absorption cross sections of $CF_3C(O)Cl$ according to Eq. (9) for temperatures from 223 to 298 K and wavelength from 218–330 nm

$a_0 = -8.8912918 \times 10^1$	$b_0 = 3.7950580$
$a_1 = 9.6418661 \times 10^{-1}$	$b_1 = -5.9114731 \times 10^{-2}$
$a_2 = -5.4370794 \times 10^{-3}$	$b_2 = 3.4406419 \times 10^{-4}$
$a_3 = 1.4975946 \times 10^{-5}$	$b_3 = -8.8699856 \times 10^{-7}$
$a_4 = -1.6768324 \times 10^{-7}$	$b_4 = 8.5483894 \times 10^{-10}$

$$\ln\sigma(\lambda,T) = (a_0 + a_1\lambda + a_2\lambda^2 + a_3\lambda^3 + a_4\lambda^4) + (b_0 + b_1\lambda + b_2\lambda^2 + b_3\lambda^3 + b_4\lambda^4)(T - T_0) \quad (9)$$

A polynomial least-squares fit of the data from Table 1 was performed with respect to temperature and wavelength λ using a program developed in this institute. Since it was impossible to fit the whole spectrum from 200 to 330 nm with this function, two separate calculations for the range 200–220 nm and 218–330 nm were performed. The resulting polynomial constants are listed in Tables 2 and 3. Comparison of the measured and calculated values shows that the deviations are smaller than 3% almost throughout the entire spectrum. Only between 220 and 230 nm (error up to 6%) and for wavelengths longer than 300 nm (error up to 20% at 330 nm) were larger deviations observed.

The only published $CF_3C(O)Cl$ UV absorption cross-section data are those of Rattigan et al. [11,12]. A dual-beam diode-array spectrometer with a spectral resolution of 1.2 nm was used to investigate the absorption cross-section for $CF_3C(O)Cl$ at different temperatures in the region 200 to 330 nm. Good agreement (less than 5% difference) exists between the two spectra at room temperature over the whole range, except for wavelengths longer than 315 nm, where cross-sections are smaller than 10^{-22} cm^2 molecule^{-1}, and in the range 215–235 nm. The discrepancies in this latter range are very large, their value at 220 nm being only 60% of that measured in this work. The relative deviations in the two sets of cross-sections are shown in Fig. 4. Rattigan et al. [12] believe that inaccuracies in the cross-section measurements in the short-wavelength region ($\lambda < 220$ nm) arise because of the low light levels transmitted by the optical fibres used in their apparatus. This does not explain, however, the discrepancies for wavelengths up to 240 nm.

Rattigan et al. [12] also reported temperature gradients which are in good agreement with those measured here, except in the region 220–240 nm. Temperature gradients

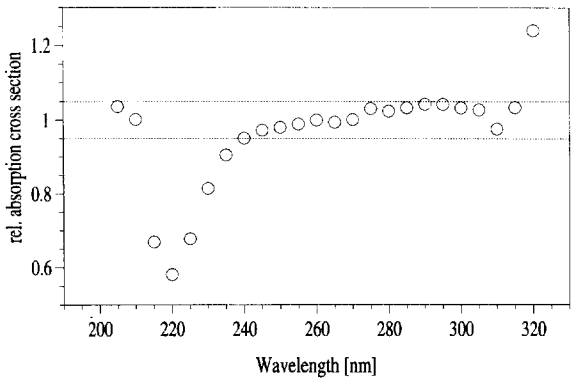

Fig. 4. Deviation of absorption cross-sections of $CF_3C(O)Cl$ measured by Rattigan et al. [12] relative to the values measured in this work. The lines represent a 5% confidence interval.

from Rattigan et al. and from this work are compared in Fig. 5. At 220 nm their value is 12 times larger than that found in this study. This discrepancy can also not be explained by low light levels transmitted by their optical fibres.

The absorption cross-section for $CF_3C(O)Cl$ at selected wavelengths are also reported in three other papers. Jemi-Alade et al. [13] reported a value of $\sigma(CF_3C(O)Cl)_{250} = 6.72 \times 10^{-20}$ cm^2 molecule^{-1} and Weibel et al. [14] give $\sigma(CF_3C(O)Cl)_{254} = (6.81 \pm 0.08) \times 10^{-20}$ cm^2 molecule^{-1}. Maricq and Szente [15] determined $\sigma(CF_3C(O)Cl)_{193} = 1.6 \times 10^{-18}$ cm^2 molecule^{-1}, $\sigma(CF_3C(O)Cl)_{248} = 5.8 \times 10^{-20}$ cm^2 molecule^{-1} and $\sigma(CF_3C(O)Cl)_{255} = 6.6 \times 10^{-20}$ cm^2 molecule^{-1} for $CF_3C(O)Cl$. The values of Jemi-Alade et al. [13], Weibel et al. [14] and the 255 nm value of Maricq and Szente [15] agree well with the cross-sections obtained here, whereas the 248 nm value of Maricq and Szente [15] seems to be unreasonably low, possibly because of a very poor signal-to-noise ratio, as can be seen in Fig. 1 of their paper.

3.2. Photolysis studies

Photolysis studies of $CF_3C(O)Cl$ have been undertaken in N_2, in air/C_2H_6 mixtures and in air in order to establish a photodissociation mechanism and to obtain quantum yields for dissociation of $CF_3C(O)Cl$, and product quantum yields

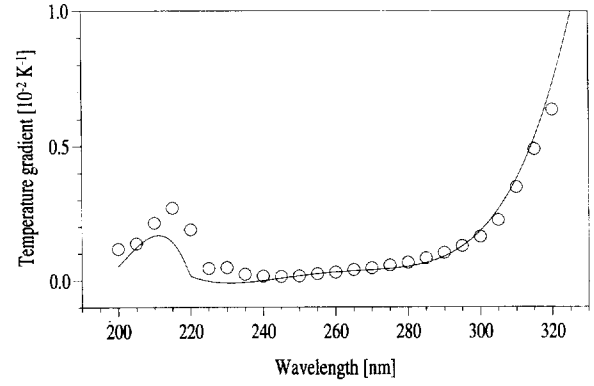

Fig. 5. Comparison of temperature gradients from this work (———) and from Rattigan et al. [12] (○).

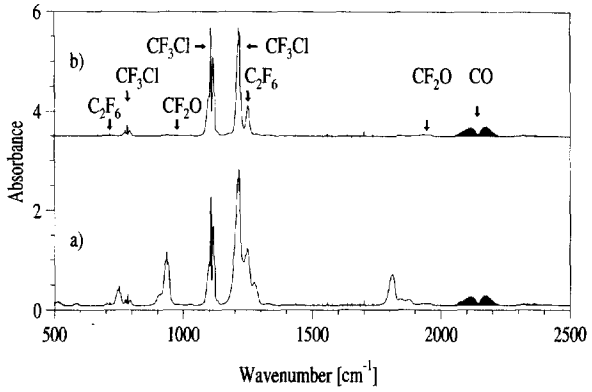

Fig. 6. (a) IR-spectrum taken after 2100 s irradiation of 3.25×10^{14} molecule cm^{-3} $CF_3C(O)Cl$ in N_2; (b) same as (a) but absorption due to $CF_3C(O)Cl$ is subtracted.

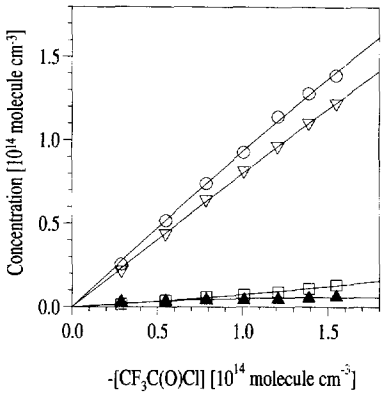

Fig. 7. Concentration of CO (○), CF_3Cl (▽), C_2F_6 (□) and CF_2O (▲) versus amount of $CF_3C(O)Cl$ consumed in the photolysis of 3.25×10^{14} molecule cm^{-3} $CF_3C(O)Cl$ in N_2.

at 254 nm. Experiments were carried out in the FTIR/photolysis apparatus at 296 K. $CF_3C(O)Cl$ concentrations ranged from $(0.95–6.66)\times10^{14}$ molecules cm^{-3} and the total pressure was adjusted to 760 torr by addition of N_2 or air. IR spectra were taken before the photolysis and after each irradiation at intervals of 300 s. The total duration of photolysis was 2100 s, during which about 50% of the initial $CF_3C(O)Cl$ was consumed. Reactant and product concentrations were calibrated against reference spectra recorded under the same conditions in the same experimental set-up.

3.3. Photolysis of $CF_3C(O)Cl$ in N_2

A total of nine photolysis experiments was carried out in N_2. A typical IR-spectrum taken after 2100 s of irradiation of 3.25×10^{14} molecule cm^{-3} $CF_3C(O)Cl$ is shown in Fig. 6(a)). For the sake of clarity, absorption due to $CF_3C(O)Cl$ has been subtracted in Fig. 6(b)). The main products of this photolysis, which can easily be determined, are CO (2050–2230 cm^{-1}), CF_3Cl (783, 1107 and 1215 cm^{-1}) and C_2F_6 (714 and 1250 cm^{-1}). Also smaller amounts of CF_2O (976 and 1944 cm^{-1}) could be detected. There is no evidence that another carbonyl compound is present. The observed concentrations and the product yields relative to the amount of $CF_3C(O)Cl$ consumed in this particular experiment are listed in Table 4 and are shown in Fig. 7. It can be seen that the main products CO and CF_3Cl increase linearly with the consumption of $CF_3C(O)Cl$ with yields of about 92 and 79%, respectively. C_2F_6 is formed with a yield of about 7%. The formation of the product CF_2O originates from the reaction initiated by CF_3+O_2 [16,17]. O_2 is present in small amounts in the photolysis cell as an impurity in N_2 and/or through very small leakages. Enhanced formation of CF_2O can be observed in the first 300 s of irradiation when the initial O_2 impurity is primarily consumed. A yield of CF_2O of about 10% is observed in the initial interval and drops down to about 4% for later photolysis intervals. In Table 5 the product yields for all the nine experiments performed in N_2 are shown. Mean values of 0.96 ± 0.04 for CO, 0.77 ± 0.04 for CF_3Cl, 0.07 ± 0.02 for C_2F_6 and 0.09 ± 0.03 for CF_2O are obtained.

As mentioned in Section 1 (Introduction), there are four possible pathways for the photodissociation of $CF_3C(O)Cl$. These reactions (Eqs. (1)–(4)) plus a number of secondary reactions can explain the formation of the products.

$$CF_3C(O)Cl+h\nu \rightarrow CF_3+CO+Cl \quad (1a)$$

$$\rightarrow CF_3C(O)+Cl \quad (2a)$$

$$\rightarrow CF_3+C(O)Cl \quad (3a)$$

$$\rightarrow CF_3Cl+CO \quad (4a)$$

Reactions involving possible radical products are quite well known. $CF_3C(O)$ and C(O)Cl dissociate under these

Table 4
Measured concentrations (molecule cm^{-3}) of $CF_3C(O)Cl$, CO, CF_3Cl, C_2F_6 and CF_2O before and during the photolysis of 3.30×10^{14} molecule cm^{-3} $CF_3C(O)Cl$ in N_2, and product yields (Y) relative to the amount of $CF_3C(O)Cl$ consumed

Time (s)	$[CF_3C(O)Cl]$	[CO]	$[CF_3Cl]$	$[C_2F_6]$	$[CF_2O]$	$Y(CO)$	$Y(CF_3Cl)$	$Y(C_2F_6)$	$Y(CF_2O)$
0	3.30×10^{14}	–	–	–	–	–	–	–	–
300	3.01×10^{14}	2.55×10^{13}	2.16×10^{13}	1.72×10^{12}	3.23×10^{12}	0.889	0.753	0.060	0.113
600	2.75×10^{14}	5.17×10^{13}	4.36×10^{13}	3.81×10^{12}	3.78×10^{12}	0.942	0.795	0.069	0.069
900	2.51×10^{14}	7.40×10^{13}	6.40×10^{13}	6.07×10^{12}	4.50×10^{12}	0.940	0.813	0.077	0.057
1200	2.29×10^{14}	9.26×10^{13}	8.13×10^{13}	7.41×10^{12}	4.46×10^{12}	0.921	0.808	0.074	0.044
1500	2.09×10^{14}	1.14×10^{14}	9.61×10^{13}	9.01×10^{12}	5.06×10^{12}	0.946	0.797	0.075	0.042
1800	1.91×10^{14}	1.28×10^{14}	1.10×10^{14}	1.10×10^{13}	5.58×10^{12}	0.923	0.793	0.079	0.040
2100	1.75×10^{14}	1.39×10^{14}	1.22×10^{14}	1.33×10^{13}	6.55×10^{12}	0.895	0.785	0.086	0.042

Table 5
Product yields (Y) of CO, CF_3Cl, C_2F_6 and CF_2O after 2100 s irradiation relative to the amount of $CF_3C(O)Cl$ consumed in several photolysis experiments of $CF_3C(O)Cl$ at 254 nm in N_2

$[CF_3C(O)Cl]_0$ (molecule cm^{-3})	$Y(CO)$	$Y(CF_3Cl)$	$Y(C_2F_6)$	$Y(CF_2O)$
3.30×10^{14}	0.90	0.79	0.09	0.04
3.65×10^{14}	0.98	0.77	0.07	0.08
2.75×10^{14}	0.93	0.76	0.06	0.07
3.14×10^{14}	0.95	0.81	0.07	0.08
4.63×10^{14}	1.01	0.75	0.05	0.10
2.99×10^{14}	0.97	0.75	0.08	0.12
4.15×10^{14}	0.93	0.78	0.07	0.08
3.85×10^{14}	0.99	0.73	0.06	0.12
4.33×10^{14}	0.94	0.83	0.05	0.10
Mean value	0.96 ± 0.04	0.77 ± 0.04	0.07 ± 0.02	0.09 ± 0.03

experimental conditions to CF_3 and CO [18,19], and CO and Cl [20], respectively, rather than reacting with other radicals or molecules.

$$CF_3C(O)+M\rightarrow CF_3+CO+M \quad (10)$$

$$C(O)Cl+M\rightarrow CO+Cl+M \quad (11)$$

For this reason, no $CF_3C(O)$- or $C(O)Cl$-containing products are expected to be formed and a CO product yield of 1.0 is expected in these experiments. Our product yield for CO of nearly unity (0.96 ± 0.04) does support this expectation. This product yield also indicates that there is no secondary chemistry associated with CO, which would lead to other products. Only in experiments with relatively larger amounts of O_2, as indicated by increased yields of CF_2O, were traces of CO_2 detected.

The remaining products CF_3 and Cl are radicals and are thus expected to combine, forming C_2F_6, CF_3Cl and Cl_2. Cl_2 could not be determined in this experiment, since Cl_2 does not absorb in the IR.

$$2CF_3\rightarrow C_2F_6 \quad (12)$$

$$CF_3+Cl\rightarrow CF_3Cl \quad (13)$$

$$Cl+Cl+M\rightarrow Cl_2+M \quad (14)$$

There are also other possible sources of CF_3Cl, for example the photolysis reaction depicted by Eq. (4) or the reactions of CF_3 with $CF_3C(O)Cl$ or Cl_2.

$$CF_3+CF_3C(O)Cl\rightarrow CF_3Cl+CF_3C(O) \quad (15)$$

$$CF_3+Cl_2\rightarrow CF_3Cl+Cl \quad (16)$$

It will be shown later in this paper, that the photolysis reaction depicted by Eq. (4) occurs, but only to a minor extent. The abstraction of Cl by CF_3 from $CF_3C(O)Cl$ can be ruled out since the same overall quantum yields were determined in the photolysis experiments performed in N_2 and in air, where CF_3 radicals are instantaneously scavenged by O_2.

FACSIMLE calculations were performed to investigate the importance of the reactions depicted by Eqs. (13) and (16) for the formation of CF_3Cl. A simple mechanism consisting of reactions shown by Eqs. (1), (12)–(14) and (16) was used. First k_{13} was calculated by fitting the observed concentrations of CF_3Cl and C_2F_6. Using $k_{12}=1.5\times10^{-11}$ cm^3 $molecule^{-1}$ s^{-1} [21], $k_{14}=1.4\times10^{-32}$ cm^6 $molecule^{-2}$ s^{-1} [22], $k_{16}=2.9\times10^{-14}$ cm^3 $molecule^{-1}$ s^{-1} [23], a value of $k_{13}=(1.6\pm0.2)\times10^{-11}$ cm^3 $molecule^{-1}$ s^{-1} was obtained. This value is consistent with reported rate constants for reactions of CF_3 with other halogen atoms, $k_{17}=2.0\times10^{-11}$ cm^3 $molecule^{-1}$ s^{-1} for the reaction with F (Eq. (17)) atoms [24] and $k_{18}=8.7\times10^{-12}$ cm^3 $molecule^{-1}$ s^{-1} for the reaction with I atoms [25] (Eq. (18)).

$$CF_3+F\rightarrow CF_4 \quad (17)$$

$$CF_3+I\rightarrow CF_3I \quad (18)$$

Using the mechanism and rate constants mentioned above, it could also be calculated that 100 times more CF_3Cl is formed by the reaction depicted by Eq. (13) that by that depicted by Eq. (16) at the beginning of the photolysis (about 100 s after the start) and that this ratio decreases to 10 at the end of the photolysis experiments.

As already mentioned the formation of the product CF_2O is caused by a side reaction due to the presence of small amounts of O_2. The CF_3 radicals can add molecular oxygen to form CF_3O_2 radicals which will lead to CF_2O. The reaction shown by Eq. (19) and the subsequent reactions leading to the production of CF_2O, will be discussed in more detail in the section dealing with the photolysis of $CF_3C(O)Cl$ in air.

$$CF_3+O_2+M\rightarrow CF_3O_2+M \quad (19)$$

Since the formation of the product CF_2O is caused by a side reaction of CF_3 in the presence of unwanted O_2, it is legitimate to add the amount of CF_2O proportionally to CF_3Cl and C_2F_6 in order to calculate the yields of CF_3Cl and C_2F_6 in pure N_2. Yields of 0.86 ± 0.04 for CF_3Cl and 0.07 ± 0.02 for C_2F_6 can be calculated in this way. In a photolysis study of $CF_3C(O)Cl$ in inert gas by Weibel et al. [14], mean values for quantum yields between 254–280 nm are given: $\Phi_{CF_3Cl}=0.86\pm0.11$ and $\Phi_{C_2F_6}=0.062\pm0.023$. In this work values $\Phi_{CF_3Cl}=0.86\pm0.04$ and $\Phi_{C_2F_6}=0.07\pm0.02$ are obtained; these are in excellent agreement with the measurement of Weibel et al. [14].

3.4. Photolysis of $CF_3C(O)Cl$ in the presence of C_2H_6 in air

Mixtures of (3.0–3.9) $\times 10^{14}$ molecule cm^{-3} $CF_3C(O)Cl$ and (0.6–6.6) $\times 10^{15}$ molecule cm^{-3} C_2H_6 were photolysed at 254 nm in 760 torr air. The only fluorinated products detected in the IR-spectra were CF_2O (774, 976, 1255 and 1944 cm^{-1}) and HF (not displayed). Other products observed were CO (2050–2230 cm^{-1}), CO_2 (2230–2400 cm^{-1}), HCl (outside the displayed range), CH_3CHO (1122, 1760 and 2730 cm^{-1}) and at longer photolysis times HCHO (1745 and 2801 cm^{-1}), as is shown in Fig. 8. Again, in Fig. 8(a)), the absorbance spectrum after 2100 s including the unconsumed $CF_3C(O)Cl$ is shown, whereas in Fig. 8(b)) only the absorptions of the products are presented.

Fig. 9 shows the observed concentration of the products versus the amount of $CF_3C(O)Cl$ consumed in the photolysis of 3.83×10^{14} molecule cm^{-3} $CF_3C(O)Cl$ in the presence of 6.58×10^{15} molecule cm^{-3} C_2H_6 in air. In this particular experiment, as well as in the other experiments in the presence of C_2H_6, the products CF_2O and CO are formed with a constant yield of about 1.0 ± 0.1. Deviations are within experimental error. Also shown in this figure are the observed concentrations of CH_3CHO and CO_2 which show a clearly curved dependence on the amount of $CF_3C(O)Cl$ consumed.

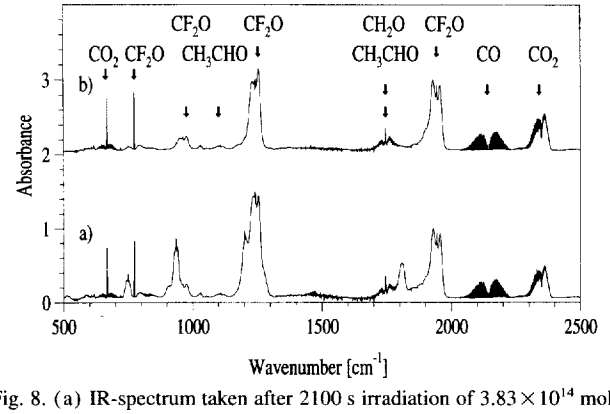

Fig. 8. (a) IR-spectrum taken after 2100 s irradiation of 3.83×10^{14} molecule cm^{-3} $CF_3C(O)Cl$ in air/C_2H_6 mixtures; (b) same as (a) but absorption due to $CF_3C(O)Cl$ is subtracted.

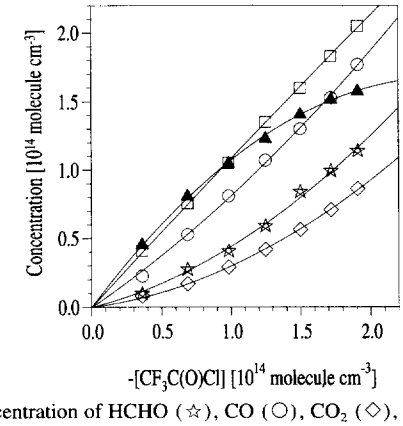

Fig. 9. Concentration of HCHO (☆), CO (○), CO_2 (◇), CF_2O (□) and CH_3CHO (▲) versus amount of $CF_3C(O)Cl$ consumed in the photolysis of 3.83×10^{14} molecule cm^{-3} $CF_3C(O)Cl$ in air/C_2H_6 mixtures.

This indicates that for both molecules secondary chemistry occurs. The yield and the shape of these curves are dependent on the initial ratio of $CF_3C(O)Cl$ and C_2H_6.

Information about primary dissociation processes can be obtained from the CO product yield. From the four possible photodissociation pathways Eqs. (1)–(4) only the pathways depicted by Eqs. (1) and (4) produce CO directly. Contributions from pathway Eq. (4) are very small since no CF_3Cl could be found in these experiments. Further dissociation of the CO-containing fragments of the photolysis pathways depicted by Eqs. (2) and (3) is only a minor pathway under these experimental conditions. In contrast with the experiments in N_2, the addition of O_2 is favoured in the presence of 760 torr air.

$$CF_3C(O) + O_2 + M \rightarrow CF_3C(O)O_2 + M \quad (20)$$

$$C(O)Cl + O_2 + M \rightarrow ClC(O)O_2 + M \quad (21)$$

The ratios of O_2 addition to the decomposition were measured by Wallington et al. [19] and by Hewitt et al. [26]. Values for $k_{20}/(k_{10}+k_{20})$ of 0.97 and for $k_{21}/(k_{11}+k_{21})$ of 0.90 are reported for similar experimental conditions. These results signify that the addition of O_2 is by far the most important reaction pathway for $CF_3C(O)$ and C(O)Cl. $CF_3C(O)O_2$ and $ClC(O)O_2$ react further via the reactions shown in Eqs. (22)–(25) leading to CO_2 and CF_3 as shown in [19], and CO_2 and Cl shown in [26], respectively.

$$2CF_3C(O)O_2 \rightarrow 2CF_3C(O)O + O_2 \quad (22)$$

$$CF_3C(O)O \rightarrow CF_3 + CO_2 \quad (23)$$

$$2ClC(O)O_2 \rightarrow 2ClC(O)O + O_2 \quad (24)$$

$$ClC(O)O \rightarrow Cl + CO_2 \quad (25)$$

If it is assumed that pathways Eq. (2) or Eq. (3) were the only photolysis steps occurring, then CO yields of less than 3% or less than 10%, respectively, would be expected. The high yield of CO is an indication that this is not the case, and that dissociation is predominantly via the pathway depicted in Eq. (1).

In order to evaluate a primary product yield for CO, other loss and formation processes need to be considered. It is known that CO oxidation processes occur in the presence of O_2 initiated by Cl or CF_3O radicals to form CO_2. The Cl-initiated oxidation of CO has been intensively studied [20,26–29].

$$Cl + CO + M \rightarrow C(O)Cl + M \quad (26)$$

Similarly, CF_3O also adds CO. Varetti and Aymonino [30] reported the nearly quantitative oxidation of CO in the photolysis of CF_3OF in the presence in O_2. They found that photochemically generated CF_3O radicals react with CO to form $CF_3OC(O)$, which in air add O_2 to yield $CF_3OC(O)O_2$. The last compound is most likely to react with another peroxy radical (e.g. self reaction). The $CF_3OC(O)O$ radicals formed are expected to dissociate and regenerate CF_3O. This pre-

dicted chain mechanism was confirmed in another study performed in this laboratory [31].

$$CF_3O + CO \rightarrow CF_3OC(O) \quad (27)$$

$$CF_3OC(O) + O_2 (+M) \rightarrow CF_3OC(O)O_2 (+M) \quad (28)$$

$$2CF_3OC(O)O_2 \rightarrow 2CF_3OC(O)O + O_2 \quad (29)$$

$$CF_3OC(O)O \rightarrow CF_3O + CO_2 \quad (30)$$

Under the experimental conditions (presence of excess C_2H_6) Cl and CF_3O radicals are successfully scavenged by the C_2H_6, so that no secondary chemistry consuming CO takes place.

Photolysis of CH_3CHO, the main product from the ethane scavenging reactions, also takes place in this system via the reactions shown in Eqs. (31)–(33) and has to be considered as a possible source of CO. The quantum yields of CH_3CHO at 254 nm for pathways Eqs. (31)–(33) are approximately 0.50, 0.25 and 0.23, respectively [32] and the absorption cross-section at 254 nm ($\sigma(CH_3CHO)_{254} = 1.60 \times 10^{-20}$ cm^2 $molecule^{-1}$ [33]) is about five times smaller than that of $CF_3C(O)Cl$.

$$CH_3CHO + h\nu \rightarrow CH_4 + CO \quad (31)$$

$$\rightarrow CH_3 + CHO \quad (32)$$

$$\rightarrow CH_3CO + H \quad (33)$$

CO is produced directly by the reaction shown in Eq. (31) and in the secondary reaction of O_2 with the CHO produced in the pathway depicted in Eq. (32) (see Eq. (34)). No CO is expected from the further oxidation of the CH_3CO produced in Eq. (33).

$$CHO + O_2 \rightarrow CO + HO_2 \quad (34)$$

HCHO, which is observed at longer photolysis times, is not a possible source of CO since the absorption cross-section of HCHO at 254 nm (exactly 253.65 nm) is very low ($\sigma(HCHO)_{254} = 2.92 \times 10^{-21}$ cm^2 $molecule^{-1}$ [34]) and H abstraction reactions with Cl or CF_3O are negligible because of the large excess of C_2H_6.

The total amount of CO formed versus the amount of $CF_3C(O)Cl$ photolyzed is shown in Fig. 10. From all experiments performed, a mean value for the CO product yield of 0.99 ± 0.03 was obtained from the slope. However, in order to obtain the primary CO product yield from the photolysis of $CF_3C(O)Cl$, corrections for the amount of CO formed in the photolysis of CH_3CHO need to be performed. If the amounts of CO formed in the CH_3CHO photolysis at 254 nm are subtracted from the observed concentrations and the primary product yield for CO redetermined as described before, a value of $\Phi_{CO} = 0.88 \pm 0.03$ is obtained.

This result indicates that the pathways depicted by Eq. (2) and/or Eq. (3) contribute to about 12% to the total photolysis of $CF_3C(O)Cl$. This study could not distinguish between these channels. Maricq and Szente [15] give a product yield of 0.86 for CO from the 248 nm photolysis of $CF_3C(O)Cl$;

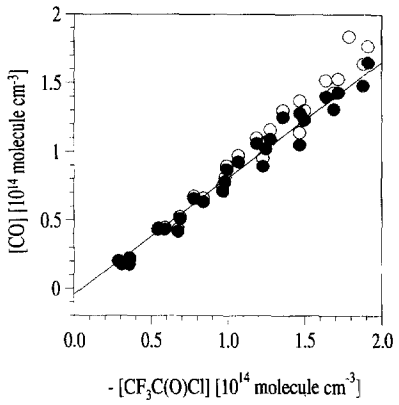

Fig. 10. Concentration of CO versus amount of $CF_3C(O)Cl$ consumed in all photolysis experiments of $CF_3C(O)Cl$ in air/C_2H_6 mixtures. Open symbols represent the measured total CO concentration and filled symbols represent the CO concentrations corrected for the additional CO generated in the CH_3CHO photolysis.

this is in excellent agreement with our result. They obtained this value from the ratio of HCl (from the reaction $Cl + C_2H_6$) and CO immediately after a laser flash. At 192 nm they found equal amounts of HCl and CO. They explained their observation at 248 nm by the argument that the C–Cl bond breaks first, leaving sufficient internal excitation for the $CF_3C(O)$ fragment to dissociate in most cases.

3.5. Photolysis of $CF_3C(O)Cl$ in air

When $CF_3C(O)Cl$ in 760 torr synthetic air is photolyzed at 254 nm, the products CO (2050–2230 cm^{-1}), CO_2 (2230–2400 cm^{-1}), CF_2O (774, 976 and 1944 cm^{-1}) and $CF_3O_3CF_3$ (1170, 1254 and 1290 cm^{-1}) were easily identified by their IR spectra, as can be seen in Fig. 11. $CF_3O_2CF_3$ and CF_3Cl were identified as products after trapping the product mixture at 77 K and fractional distillation. The fraction boiling at 191 K showed the typical absorption features of CF_3Cl and $CF_3O_2CF_3$ after stripping the CF_2O absorptions as shown in Fig. 12. Quantitative determination of CF_3Cl was

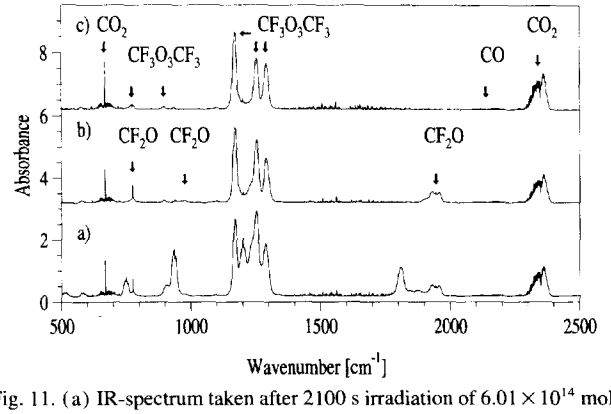

Fig. 11. (a) IR-spectrum taken after 2100 s irradiation of 6.01×10^{14} molecule cm^{-3} $CF_3C(O)Cl$ in air; (b) same as (a) but absorption due to $CF_3C(O)Cl$ is subtracted, (c) same as (b) but absorption due to CF_2O is subtracted.

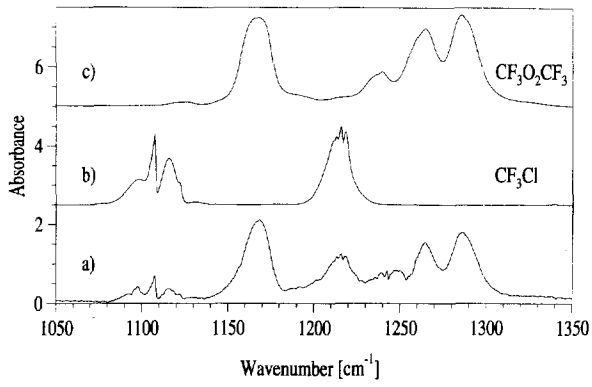

Fig. 12. (a) IR-spectrum of the 191 K fraction in the distillation of the products of the photolysis of 1.0×10^{16} molecule cm^{-3} $CF_3C(O)Cl$; (b) reference spectrum of CF_3Cl and (c) reference spectrum of $CF_3O_2CF_3$.

not possible using this method because complete transfer (freezing and distilling) could not be achieved. The CF_3Cl yield was only estimated to be less than 0.005 based on the absorbance in the IR-spectra taken directly after the photolysis. The formation of the fully halogenated compound CF_3Cl is very crucial because it is affecting the ODP of the parent compound CF_3CCl_2H.

All other products were quantitatively determined from the photolysis experiments in air. In Fig. 13 the concentrations of the products relative to the amount of $CF_3C(O)Cl$ consumed are shown for an experiment with an initial $CF_3C(O)Cl$ concentration of 6.04×10^{14} molecule cm^{-3}. It can be seen that the fluorinated products CF_2O and $CF_3O_3CF_3$ are formed with constant yield over the duration of the irradiation, indicating that no secondary chemistry is interfering with product formation. At longer photolysis times, however, the formation rate of $CF_3O_3CF_3$ appears to slow down. This is due to slight absorption and photolysis of $CF_3O_3CF_3$ at 254 nm [5]. Concentrations for $CF_3O_2CF_3$, which are not shown in this plot, were determined in a few experiments only. Concentrations of $CF_3O_2CF_3$ were found to be 25–35% of the amount of $CF_3O_3CF_3$.

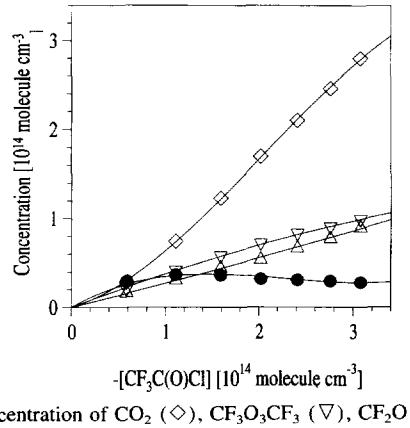

Fig. 13. Concentration of CO_2 (◇), $CF_3O_3CF_3$ (▽), CF_2O (△) and CO (●) versus amount of $CF_3C(O)Cl$ consumed in the photolysis of 5.00×10^{14} molecule cm^{-3} $CF_3C(O)Cl$ in air.

The main initial product is CO, which shows different behaviour. It reaches its concentration maximum in the third interval, followed by a concentration decrease at longer photolysis times. The observed CO yield after 300 s is about 0.5, but drops to about 0.1 at the end of the photolysis. Since the initial CO yield is close to unity, as was deduced from the experiments in air/C_2H_6 mixtures, the actual removal of CO may indicate that indeed Cl and/or CF_3O radicals are responsible for the loss of CO. The behaviour of CO_2 is the opposite to that of CO. After an induction period, the CO_2 formation rate accelerates towards the end of the experiment. The behaviour of CO is typical for a primary product which is consumed by secondary chemistry, whereas the CO_2 product is formed only by secondary chemistry. The shape of the CO concentration profile changes with the initial concentration of $CF_3C(O)Cl$. As the initial concentration of $CF_3C(O)Cl$ is increasing, the observed CO yield at $t = 300$ s decreases and the maximum of the CO concentration is reached sooner.

It was also found that the ratio of CF_2O to $CF_3O_3CF_3$ is also dependent on the initial $CF_3C(O)Cl$ concentration. For the highest initial $CF_3C(O)Cl$ concentration used, CF_2O and $CF_3O_3CF_3$ are formed in nearly equal amounts, whereas for low initial $CF_3C(O)Cl$ concentration the formation of CF_2O dominates. This can be explained by the fact that at high $CF_3C(O)Cl$ concentration, and consequently also a high photolysis rate and higher radical concentration, the formation of $CF_3O_3CF_3$ is favoured over CF_2O formation according to the following mechanism:

$$CF_3 + O_2 + M \rightarrow CF_3O_2 + M \quad (19)$$

$$2CF_3O_2 \rightarrow 2CF_3O + O_2 \quad (35)$$

$$\rightarrow CF_3O_2CF_3 + O_2 \quad (36)$$

$$CF_3O + CF_3O_2 \rightarrow CF_3O_3CF_3 \quad (37)$$

$$CF_3O + CF_3O \rightarrow CF_3O_2CF_3 \quad (38)$$

$$CF_3O + \text{wall} \rightarrow CF_2O \quad (39)$$

Thermal decomposition of CF_3O via Eq. (40) or the reaction of CF_3O with O_2 (Eq. (41)) are not possible since both reactions are endothermic by 25.2 kcal mol^{-1} and ~ 10 kcal mol^{-1}, respectively [35,36]. Known reactions of the CF_3O radical with NO to form CF_2O and FNO (Eq. (42)) [36–39] or with hydrocarbons and the subsequent decomposition of the formed CF_3OH (Eqs. (43) and (44)) [40,41] can be ruled out, since neither NO nor hydrocarbons are present in this system. Therefore it is believed that CF_2O is formed by surface-catalysed decomposition of the CF_3O radical (Eq. (41)) as indicated in other studies [42,43].

$$CF_3O \rightarrow CF_2O + F \quad (40)$$

$$CF_3O + O_2 \rightarrow CF_2O + FO_2 \quad (41)$$

$$CF_3O + NO \rightarrow CF_2O + FNO \quad (42)$$

$$CF_3O + RH \rightarrow CF_3OH + R \quad (43)$$

$$CF_3OH \rightarrow CF_2O + HF \quad (44)$$

3.6. Quantum yield for dissociation

Quantum yields for dissociation of $CF_3C(O)Cl$ at 254 nm were determined for all the experiments described above (in N_2, in C_2H_6/air mixtures and in air) using CCl_2O as an actinometer. CCl_2O was chosen since it absorbs in the same wavelength region with absorption cross-sections close to those of $CF_3C(O)Cl$ [44]. Separate photolysis experiments of CCl_2O in 760 torr air were performed frequently between the $CF_3C(O)Cl$ photolysis experiments.

A photolysis rate constant for CCl_2O of $k(CCl_2O)_{254} = (3.18 \pm 0.20) \times 10^{-4}\ s^{-1}$ was determined. A photolysis rate constant of $k(CF_3C(O)Cl)_{254} = (3.41 \pm 0.13) \times 10^{-4}\ s^{-1}$ was calculated for the photolysis experiments of $CF_3C(O)Cl$ at 254 nm in 760 torr N_2, air or C_2H_6/air mixtures. Using the absorption cross-sections for CCl_2O, $\sigma(CCl_2O)_{254} = 6.36 \times 10^{-20}$ cm^2 molecule^{-1} [44], and for $CF_3C(O)Cl$, $\sigma(CF_3C(O)Cl)_{254} = 6.86 \times 10^{-20}$ cm^2 molecule^{-1} (measured in the present work) at 254 nm, and using a quantum yield of unity of CCl_2O [45], the quantum yield for the dissociation of $CF_3C(O)Cl$ was calculated using Eq. (45) to be $\Phi(CF_3C(O)Cl)_{254} = 0.95 \pm 0.05$. The error was calculated using the experimental scattering of all six runs for the photolysis rate constants and an error of 3% for the absorption cross-sections.

$$\Phi(CF_3C(O)Cl)_{254} = \Phi(CCl_2O)_{254} \frac{k(CF_3C(O)Cl)_{254}\sigma(CCl_2O)_{254}}{k(CCl_2O)_{254}\sigma(CF_3C(O)Cl)_{254}} \quad (45)$$

In order to determine the pressure-dependence of $\Phi(CF_3C(O)Cl)_{254}$, several photolysis experiments of $(2.82\text{–}3.43) \times 10^{14}$ molecule cm^{-3} $CF_3C(O)Cl$ were performed in air at total pressures between 50 and 760 torr. Quantum yields, determined in the same way as described above, ranged from 1.00 to 1.06. In Fig. 14 the quantum yields are plotted versus the total pressure. No obvious change in the quantum yield was observed within the pressure range and thus the quantum yields are not pressure-dependent.

Our results are in very good agreement with the quantum yield, presented by Maricq and Szente [15], of $\Phi_{248} = 0.92 \pm 0.08$ for dissociation at 248 nm in 120 torr O_2/N_2 mixtures and the value of $\Phi_{254} = 0.98 \pm 0.13$ obtained at 254 nm in c-C_4F_8 at pressures up to 535.2 torr by Weibel et al. [14]. No pressure-dependence was observed by Weibel et al. [14] in the pressure range 66 to 535 torr.

3.7. Cl_2 quantum yield

Since molecular chlorine does not absorb in the infrared, analysis of Cl_2 was performed in the ultraviolet. During the photolysis of $CF_3C(O)Cl$, the transmitted light was monitored with a resolution of 1 nm at $\lambda = 330$ nm by means of a photomultiplier. Fig. 15 shows the change in the photomultiplier signal due to Cl_2 formation recorded in a typical experiment. After filling the cell (up to 250 s), I_0 was measured for 350 s. During the irradiation the photomultiplier signal decreases because of the Cl_2 formation. At 600 s photolysis was started for a period of 1800 s. I_{end} was registered for another 350 s before pumping out the cell. The signal returns to the value I_0 before filling the cell, indicating that the output of the light source did not change with time.

Photolysis experiments were performed using six samples of $(4.07\text{–}9.07) \times 10^{14}$ molecules cm^3 $CF_3C(O)Cl$ in 760 torr air. The concentration of Cl_2 formed was calculated from Eq. (46) using $\sigma(Cl_2)_{330} = 2.55 \times 10^{-19}$ cm^2 molecule^{-1} [46] and $l = 982$ cm. The concentration of $CF_3C(O)Cl$ before and after irradiation was determined by infrared analysis.

$$[Cl_2] = \ln(I_0/I_{end})/l\sigma(Cl_2) \quad (46)$$

The initial concentration of $CF_3C(O)Cl$ and the photomultiplier signals before and after the irradiation are given in Table 6 for the six experiments. Also presented are the calculated Cl_2 concentrations, the amounts of $CF_3C(O)Cl$ removed and the resulting Cl_2 quantum yield. The mean value for the quantum yield of Cl_2 determined in these experiments is $\Phi_{Cl_2} = 0.502 \pm 0.012$ indicating that all chlorine originating from $CF_3C(O)Cl$ is converted into molecular chlorine.

Cl_2 quantum yields were reported in two previous studies. Rattigan et al. [11,12] found that the amount of Cl_2 produced was quantitatively equal to 0.50 times the amount of

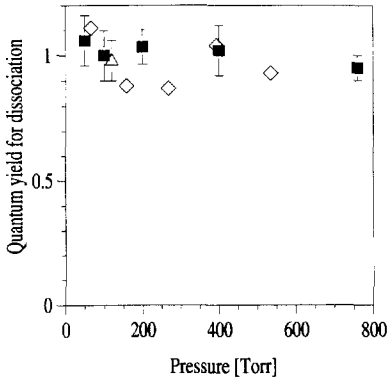

Fig. 14. Quantum yield for dissociation of $CF_3C(O)Cl$ at 254 nm versus total pressure obtained in this work (■) compared with data of Maricq and Szente [15] (△) and Weibel et al. [14] (◇).

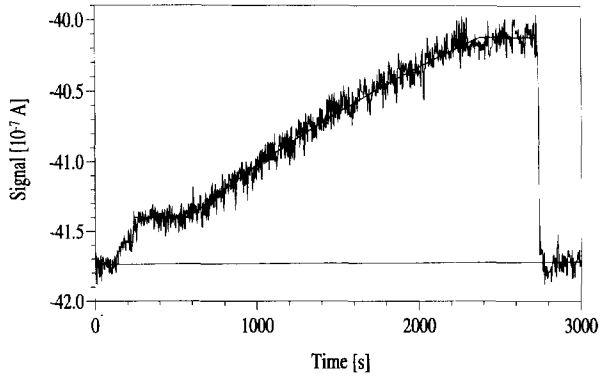

Fig. 15. Photomultiplier signal recorded in a typical experiment ($[CF_3C(O)Cl]_0 = 5.34 \times 10^{14}$ molecule cm^{-3}) for determining the Cl_2 concentration in the photolysis of $CF_3C(O)Cl$ in air.

Table 6
Experiments for the determination of the Cl_2 quantum yield at 254 nm in the photolysis of $CF_3C(O)Cl$ in 760 torr air

$[CF_3C(O)Cl]_0$ (molecule cm^{-3})	I_0 (A)	I_{end} (A)	$[Cl_2]$ (molecule cm^{-3})	$D[CF_3C(O)Cl]$ (molecule cm^{-3})	Φ_{Cl_2}
5.34×10^{14}	-4.140×10^{-6}	-4.012×10^{-6}	1.25×10^{14}	2.45×10^{14}	0.509
9.07×10^{14}	-4.127×10^{-6}	-3.916×10^{-6}	2.09×10^{14}	4.16×10^{14}	0.501
4.07×10^{14}	-4.125×10^{-6}	-4.026×10^{-6}	9.65×10^{13}	1.87×10^{14}	0.517
5.11×10^{14}	-4.116×10^{-6}	-4.000×10^{-6}	1.14×10^{14}	2.34×10^{14}	0.485
4.83×10^{14}	-4.104×10^{-6}	-3.993×10^{-6}	1.09×10^{14}	2.22×10^{14}	0.492
4.60×10^{14}	-4.105×10^{-6}	-3.996×10^{-6}	1.07×10^{14}	2.11×10^{14}	0.507

$CF_3C(O)Cl$ consumed, and Hayman et al. [2] reported a production of an equivalent amount of Cl_2 from the photolysis of $CF_3C(O)Cl$ in the presence of HCl in air.

3.8. Photodissociation rate constants and atmospheric implications

The atmospheric photodissociation rate constants were calculated by use of Eq. (47)

$$J(\Theta,z) = \int \sigma(\lambda)\Phi(\lambda)I(\lambda,\Theta,z)\mathrm{d}\lambda \quad (47)$$

$J(\Theta,z)$ is the photodissociation rate constant as a function of zenith angle Θ and altitude z; $\sigma(\lambda)$ is the absorption cross-section as a function of wavelength λ; $I(\lambda,\Theta,z)$ is the actinic flux as a function of wavelength λ, zenith angle Θ and altitude z as used in previous calculations [32,47]; Φ is the quantum yield for dissociation. Φ was determined in this work as unity. The actinic flux parameters were based on the radiation transfer model by Luther and Gelinas [48].

The photodissociation rate-constants calculated with the temperature-dependent absorption cross-sections are given in Fig. 16 as a function of altitude for three zenith angles (0, 50 and 70°). Photodissociation rate constants obtained at ground level are also presented as a function of zenith angle in Fig. 17. In this figure photodissociation rate constants for $CF_3C(O)Cl$ are compared with values calculated for HCHO [34]. In order to compare these results with those from with other models, we also calculated $J_{HCHO} = 4.2\times10^{-4}\ s^{-1}$ (see Fig. 5), which can be used as a 'reference molecule' to compensate for the difference in the employed models.

In the troposphere and the lower stratosphere (below 15 km), where photolysis occurs only at wavelengths longer than 295 nm, the temperature-dependence of the absorption cross-section plays an important role in the calculation of the photodissociation rate-constant. As the absorption cross-section decreases with decreasing temperature and the light intensity increases with increasing altitude, the calculated photodissociation rate constant remains nearly unchanged in the troposphere up to 10 km. For zenith angles of 20–50° the J-value is about $2\text{–}3\times10^{-7}\ s^{-1}$, this represents a tropospheric lifetime for photolysis of about 40 to 60 days under noon conditions.

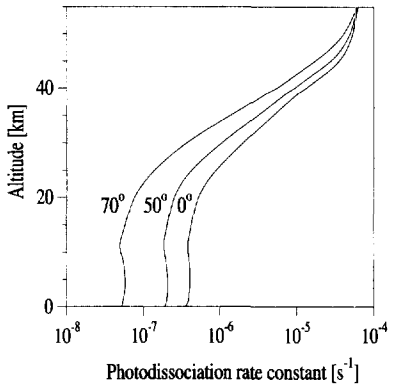

Fig. 16. Photodissociation rate-constants of $CF_3C(O)Cl$ as a function of altitude for different zenith angles.

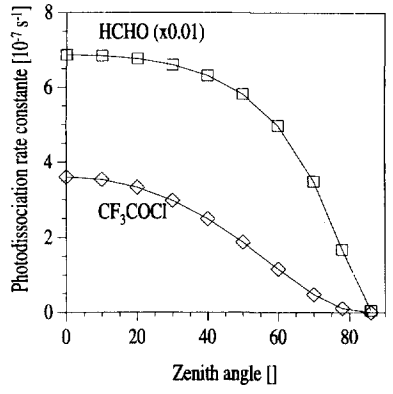

Fig. 17. Comparison of photodissociation rate-constants of CF_3CCl and HCHO as a function of zenith angle at ground level.

Rattigan et al. [11] calculated a globally averaged photolysis lifetime of 33 days for $CF_3C(O)Cl$. Hayman et al. [2] cited Rattigan et al. [12] to report an upper tropospheric lifetime of 86 days with respect to loss by photolysis, a value that they confirmed in their modelling studies. More recently, in the modelling study on CFC replacement compounds by Wild et al. [49] an annual mean global tropospheric photolysis lifetime of $CF_3C(O)Cl$ of 56.4 days was calculated. The disagreement between these studies might be caused by different models used (box model or 2D model) and different assumptions made (e.g. albedo, temperature or global distribution of the species).

Acknowledgements

The authors wish to thank the Commission of the European Communities for financial support (EV 5V-CT-91-0024).

References

[1] World Meteorological Organization, Global Ozone Research and Monitoring Project-Report no. 20 Scientific Assessment of Stratospheric Ozone: 1989, Vol. 2, Appendix: AFEAS report, (1989).
[2] G.D. Hayman, M.E. Jenkins, T.P. Murrels, C.E. Johnson, Atmos. Environ. 28 (1993) 421.
[3] T.J. Wallington, W.F. Schneider, D.R. Worsnop, O.J. Nielsen, J. Sehested, W.J. Debruyn, J.A. Shorter, Environ. Sci. Technol. 28 (1994) 320A.
[4] R. Meller, D. Boglu, G.K. Moortgat, Proc. STEP HALOCSIDE/AFEAS Workshop, Dublin, 1991, 110-115.
[5] R. Meller, W. Raber, J.N. Crowley, M.E. Jenkin, G.K. Moortgat, J. Photochem. Photobiol. A: Chem. 62 (1991) 163.
[6] D. Bauer, J.N. Crowley, G.K. Moortgat, J. Photochem. Photobiol. A: Chem. 65 (1992) 329.
[7] W.H. Raber, G.K. Moortgat, in: Progress and Problems in Atmospheric Chemistry, J. Barker (Ed.), World Scientific Publ. Co, Singapore, 1996, 318-373.
[8] L.R. Anderson, W.B. Fox, J. Am. Chem. Soc. 89 (1967) 4313.
[9] R. Meller, G.K. Moortgat, J. Photochem. Photobiol. A: Chem. 86 (1995) 15.
[10] D. Gillotay, P.C. Simon, J. Atmos. Chem. 12 (1991) 269.
[11] O. Rattigan, R.A. Cox, R.L. Jones, Proc. STEP HALOCSIDE/AFEAS Workshop, Dublin, 1991, 116-125.
[12] O.V. Rattigan, O. Wild, R.L. Jones, R.A. Cox, J. Photochem. Photobiol. A: Chem. 73 (1993) 1.
[13] A.A. Jemi-Alade, P.D. Lightfoot, R. Lesclaux, Chem. Phys. Lett. 179 (1991) 119.
[14] D.E. Weibel, G.A. Arguello, E.R. de Staricco, E.H. Staricco, J. Photochem. Photobiol. A: Chem. 86 (1995) 27.
[15] M.M. Maricq, J.J. Szente, J. Phys. Chem. 99 (1995) 4554.
[16] O.J. Nielsen, T. Ellermann, J. Sehested, E. Bartkiewicz, T.J. Wallington, M.D. Hurley, Int. J. Chem. Kin. 24 (1992) 1009.
[17] J. Czarnowski, H.J. Schumacher, Z. Physik. Chem. Neue Folge 92 (1974) 329.
[18] J.C. Amphlett, E. Whittle, Trans. Faraday Soc. 63 (1967) 80.
[19] T.J. Wallington, M.D. Hurley, O.J. Nielsen, J. Sehested, J. Phys. Chem. 98 (1994) 5686.
[20] J.M. Nicovich, K.D. Kreutter, P.H. Wine, J. Chem. Phys. 92 (1990) 3539.
[21] T. Ogawa, G.A. Carlson, G.C. Pimentel, J. Phys. Chem. 74 (1970) 2090.
[22] C.J. Weng, T.I. Ho, T.M. Su, J. Phys. Chem. 91 (1987) 5235.
[23] J.C. Amphlett, E. Whittle, Trans. Faraday Soc. 62 (1966) 1662.
[24] I.C. Plumb, K.R. Ryan, Plasma Phys. Plasma Chem. 6 (1986) 11.
[25] C.J. Cobos, J. Troe, Chem. Phys. Lett. 113 (1985) 419.
[26] A.D. Hewitt, K.M. Brahan, G.D. Boone, S.A. Hewitt, Int. J. Chem. Kin., 28 (1996) 763..
[27] H.J. Schumacher, G. Stieger, Z. Physik. Chem. B 13 (1931) 169.
[28] G.K. Rollefson, C.W. Montgomery, J. Am. Chem. Soc. 55 (1933) 4036.
[29] T. Ohta, Bull. Chem. Soc. Jpn. 56 (1983) 869.
[30] E.L. Varetti, P.J. Aymonino. An. As. Quim. Arg. 55 (1967) 153.
[31] R. Meller, G.K. Moortgat, submitted for publication.
[32] G.K. Moortgat, P. Warneck, in: R. Jaenicke (Ed.), Atmosphärische Spurenstoff, DFG, SFB-Final Report, VCH, Weinheim, 1986, 77.
[33] W. Schneider, G.K. Moortgat, 1990, Int. J. Chem. Kin., in press.
[34] R. Meller, Diplom-Thesis, Johannes–Gutenberg–Universität, Mainz, 1990.
[35] Z. Li, J.S. Francisco, J. Am. Chem. Soc. 111 (1989) 5660.
[36] T.J. Bevilacqua, D.R. Hanson, C.J. Howard, J. Phys. Chem. 97 (1993) 3570.
[37] J. Chen, T. Zhu, H. Niki, J. Phys. Chem. 96 (1992) 6115.
[38] N.R. Jensen, D.R. Hanson, C.J. Howard, J. Phys. Chem. 98 (1994) 8574.
[39] A.A. Turnipseed, S.B. Barone, A.R. Ravishankara, J. Phys. Chem. 98 (1994) 4594.
[40] J. Chen, T. Zhu, H. Niki, G.J. Mains, Geophys. Res. Lett. 19 (1992) 2215.
[41] J. Sehested, T.J. Wallington, Environ. Sci. Technol. 27 (1993) 146.
[42] O.J. Nielsen, T. Ellermann, J. Sehested, E. Bartkiewicz, T.J. Wallington, M.D. Hurley, Int. J. Chem. Kin. 24 (1992) 1009.
[43] J. Czarnowski, H.J. Schumacher, Z. Physik. Chem. Neue Folge 92 (1974) 329.
[44] W. Schneider, G.K. Moortgat, 1989, unpublished results.
[45] W.B. DeMore, S.P. Sander, D.M. Golden, R.F. Hampson, M.J. Kurylo, C.J. Howard, A.R. Ravishankara, C.E.Kolb, M.J. Molina, Chemical Kinetics and Photochemical Data for Use in Stratospheric Modelling, JPL Publication, 94-26, 1994.
[46] D. Maric, J.P. Burrows, R. Meller, G.K. Moortgat, J. Photochem. Photobiol. A: Chem. 70 (1993) 205.
[47] A. Nölle, H. Heydtmann, R. Meller, G.K. Moortgat, Geophys. Res. Lett. 20 (1993) 281.
[48] F.M. Luther, R.J. Gelinas, J. Geophys. Res. 81 (1976) 1125.
[49] O. Wild, O. Rattigan, R.I. Jones, J.A. Pyle, R.A. Cox, J. Atm. Chem. 25 (1996) 167.